Applied Physics Letters

Enhanced emission of quantum dots embedded within the high-index dielectric regions of photonic crystal slabs

Cite as: Appl. Phys. Lett. **108**, 171108 (2016); https://doi.org/10.1063/1.4948379
Submitted: 29 January 2016 • Accepted: 18 April 2016 • Published Online: 29 April 2016

Gloria G. See, Matt S. Naughton, Lu Xu, et al.

Enhanced emission of quantum dots embedded within the high-index dielectric regions of photonic crystal slabs

Gloria G. See,[1] Matt S. Naughton,[2] Lu Xu,[3] Ralph G. Nuzzo,[3] Paul J. A. Kenis,[2] and Brian T. Cunningham[1,4,a)]

[1]*Department of Electrical and Computer Engineering, Micro and Nanotechnology Laboratory, University of Illinois at Urbana-Champaign, 208 North Wright Street, Urbana, Illinois 61801, USA*
[2]*Department of Chemical and Biomolecular Engineering, University of Illinois at Urbana-Champaign, Roger Adams Laboratory, 600 South Mathews Avenue, Urbana, Illinois 61801, USA*
[3]*Department of Chemistry, University of Illinois at Urbana-Champaign, 600 South Mathews Avenue, Urbana, Illinois 61801, USA*
[4]*Department of Bioengineering, University of Illinois at Urbana-Champaign, 1270 Digital Computer Laboratory, MC-278, Urbana, Illinois 61801, USA*

(Received 29 January 2016; accepted 18 April 2016; published online 29 April 2016)

We demonstrate a method for combining sputtered TiO_2 deposition with liquid phase dip-coating of a quantum dot (QD) layer that enables precise depth placement of QD emitters within a high-index dielectric film, using a photonic crystal (PC) slab resonator to demonstrate enhanced emission from the QDs when they are located at a specific depth within the film. The depth of the QDs within the PC is found to modulate the resonant wavelength of the PC as well as the emission enhancement efficiency, as the semiconducting material embedded within the dielectric changes its spatial overlap with the resonant mode. *Published by AIP Publishing.*
[http://dx.doi.org/10.1063/1.4948379]

Since their introduction by Yablonovitch,[1] photonic crystals (PCs) have been adopted for a broad range of applications that include optical filters,[2] biosensors,[3] and photodetectors.[4] In addition to passive optical components, PCs have proven to be useful within light-emitting devices, where their dispersion can be used to increase the efficiency of photon extraction from light emitting diodes (LEDs)[5–8] or to enhance the excitation intensity of embedded photon emitters such as fluorescent dyes or quantum dots (QDs).[9–12] Photon-emitting devices that contain QDs are gaining importance for applications in lighting and video display due to their high quantum efficiency, lack of photobleaching, and availability of many emission wavelengths that can be combined to engineer a specific overall spectral output. However, due to the high fabrication cost of QDs in comparison with conventional phosphors, it is highly desirable to utilize them efficiently through development of device structures that can optimally place them within regions where their output is optimally extracted.

The structure of a PC consists of a periodic variation of high and low refractive index materials. Through appropriate design choices for the feature sizes and material properties, it is possible to tune the optical and electromagnetic properties to enable a wide range of applications. In particular, when a PC is designed to operate as a guided mode resonant filter, regions of increased energy density within the structure at the resonant wavelength can be used to amplify the excitation power experienced by photon emitters that are located within the electromagnetic field standing wave.

In this work, we demonstrate a fabrication approach that enables QDs to be incorporated within a narrow cross section of the high-index dielectric thin film and within the spatial volume of an optical standing wave mode of the PC resonant slab. The QDs experience greater electric fields for excitation from their electronic ground state, and are also optimally placed so that their emission can be extracted most efficiently in the direction normal to the PC slab surface.[13] We use a dip-coating method to apply a distinct, monolayer-scale film of QDs, and show that judicious placement of the QD "slice" within the high-index dielectric film is necessary to optimize the enhanced extraction factor. In addition, we show an increase of 3–5 times greater QD emission from within a PC, as compared with the intensity measured from a QD layer that is not embedded within a PC. This emission enhancement is as high as 8 times for off-normal output angles.

There are numerous applications that have benefited from embedding QDs within dielectric materials. Dielectric microcavities can provide mode control of QD emission[14] and the spontaneous emission from QDs can be controlled by embedding them in dielectric spheres of varying radii.[15,16] The incorporation of QDs into dielectric materials has also been used for charge storage in metal-oxide-semiconductor capacitors[17] and electronically erasable programmable read only memory (EEPROM)[18] for data storage applications.

Devices with distinct QD layers of 30–300 nm have been fabricated by ion beam sputtering,[19] ion implantation,[18] or spin coating onto sputtered thin films, often with a matrix material.[14,20,21] QDs can modify the dielectric susceptibility of the material they are embedded in,[22] and improve both absorption and photoelectric performance of photoelectrodes and solar cells when layered with TiO_2.[18,19,23,24] Silicon QDs embedded within a variety of amorphous matrix materials (silicon oxide, silicon nitride, and silicon carbide) have been shown to impact the effective refractive index of their host material, producing both blue and red shifts in the optical absorption spectra of the matrix material.[19,25]

a)Author to whom correspondence should be addressed. Electronic mail: bcunning@illinois.edu

For many embedded QD devices that are used in lighting or video display applications, controlled placement within the structure is crucial to achieving optimal output intensity performance. For example, in early devices demonstrating nanocrystals in LEDs, the nanocrystals were layered with organic spacers to control their position.[26] Within PCs, the QD positioning is a crucial aspect of the excitation and output emission efficiency, determining how much of the QD emission is coupled to the PC resonant modes. In PCs excited at their resonant wavelength, the electric field intensity decays exponentially with increasing distance from the surface,[27] making it desirable to keep emitters close to the structure surface or embedded within the device itself. To this end, we demonstrate a method that combines sputter deposition of dielectric material with liquid-phase dip-coating of QDs to create PCs with an embedded QD layer. The refractive index of the dielectric TiO_2 layer is altered by the presence of the QD layer, while the output efficiency of the QDs is highly dependent upon the depth of the QDs within the dielectric layer.

The device structure consists of two distinct 2D PC regions that enable side-by-side comparison of QD emission intensity from regions that either match or mismatch the PC resonant wavelength with the emission wavelength of embedded QDs. Figure 1(a) shows the regions interleaved in a checkerboard format, in which alternating regions have distinct resonance wavelengths. Each region has two orthogonal periods, as shown in the inset, and the two periods are designed to enhance both the excitation and emission wavelengths of embedded QDs.[28] For example, the 2D-PC in Region 1 of the checkerboard has a periodic variation ($\Lambda_1 = 340$ nm, 60% duty cycle) in the y-direction, and a shorter period ($\Lambda_2 = 200$ nm, 40% duty cycle) in the x-direction. The short period is designed to produce a guided mode resonance at UV wavelengths $350 < \lambda < 390$ nm used for QD excitation, while the longer period is designed to produce a resonance at the $\lambda = 615$ nm wavelength of QD emission. Region 2 of the checkerboard has a long period of $\Lambda_1 = 250$ nm in the y-direction, and a short period of $\Lambda_2 = 200$ nm (70% duty cycle) in the x-direction, where the short period is also designed to produce a guided mode resonance at the QD excitation wavelengths, but the long period produces a resonance at a wavelength of $\lambda = 480$ nm. Therefore, when QDs with an emission wavelength centered at $\lambda = 615$ nm are embedded within the entire structure, all the QDs (in both regions of the checkerboard) will be excited with a resonant enhancement effect, but only QDs within Region 1 will participate in the enhanced extraction effect.

This structure was designed using rigorous coupled wave analysis (RSoft, DiffractMod) for previous experiments to show the effects of combined excitation and extraction enhancement, and thus contained UV and visible wavelength resonances in both Regions 1 and 2.[28] Finite difference time domain electromagnetic computer simulation (Lumerical, FDTD) was used to update the design for this study so that the same PC grating dimensions and depth could be used for the replica polymer process, but the resonance wavelength of Region 1 would be tuned to the QD emission at $\lambda = 615$ nm by increasing the thickness of the TiO_2 layer. The updated model determined that a 95 nm thick layer $t = TiO_2$ ($n = 2.35$, Metricon Model 2010/M Prism Coupler) over the polymer layer ($n = 1.524$, Woolam VAS Ellipsometer) would optimize coupling to unpolarized QD emission at $\lambda = 615$ nm. This was consistent with the values extrapolated from the resonance conditions in the previous PC devices fabricated using the same grating structure but with alternate deposition thicknesses of the TiO_2 layer.[28] The transmission spectra for the model are shown in Figure 2 with device transmission spectra at each stage of deposition.

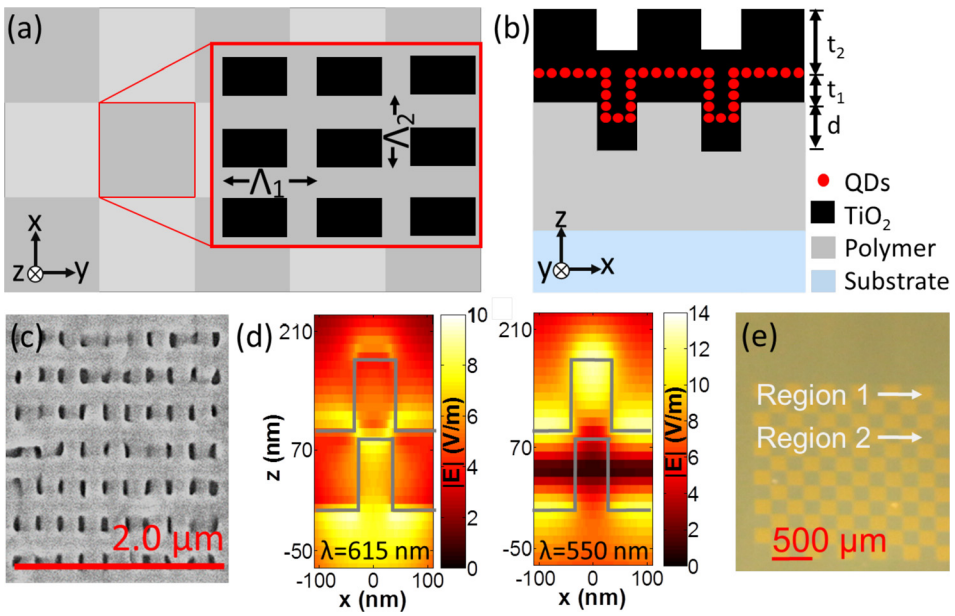

FIG. 1. (a) A top view of the device structure, consisting of two interleaved regions with different PC periods Λ_1 and Λ_2 in the *x* and *y* directions. (b) A cross-section schematic of the PC showing the replica molded polymer with a grating depth *d* and covered by thicknesses t_1 and t_2 of the TiO_2 layers sandwiching the QDs. (c) A SEM image of the PC region designed to enhance QD emission at $\lambda = 615$ nm. (d) Modeled electric field intensities for the Region 1 PC without any embedded QDs at incident wavelengths of $\lambda = 615$ nm (left) and $\lambda = 550$ nm (right), illustrating that both the wavelength and location of the QDs within the electric field will affect the enhancement conditions. (e) A photograph of QDs embedded in the checkerboard PC structure, where the orange locations show regions of enhanced emission (Region 1), while the QD emission in Region 2 and the surrounding bulk area is not enhanced.

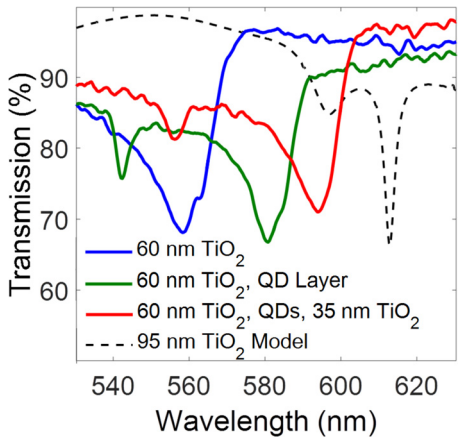

FIG. 2. The normalized transmission efficiency spectra of the PCs at various stages of fabrication and the modeled transmission spectra normalized for the 50% effective area of the checkerboard device. Each deposited layer impacts the transmission spectra of the device. The addition of a QD layer results in a resonance shift of $\lambda = 20$–25 nm and interrupts the continuous electric field within the dielectric layer, causing a change in the measured resonance conditions of the final device structure, as compared with the modeled results (shown as a dashed line). The largest dip is the resonance mode that is intended to couple with the QD emission, although additional resonances are present in the PC structure, independent of the QD emission wavelength, and are observed as shallower dips in the transmission spectra.

As mentioned previously, Region 2 has an optical resonance at $\lambda = 490$ nm, which does not overlap with the QD emission or the resonance of Region 1 at $\lambda = 615$ nm. This halves the effective device area providing QD emission enhancement. The difference in output intensity is visible to the naked eye and enables a visual confirmation of QD enhancement, as shown in the photograph of a QD embedded PC in Figure 1(e). To simplify this study, the optical characteristics near the $\lambda = 615$ nm resonance are the focus of the results presented in this work, and only one species of QD was used.

As shown in Figure 1(b), the PC has grating structure created by replicating a mold of a master structure using a UV curable polymer. A specific thickness, t_1, of TiO_2 is deposited over the replica molded polymer layer. A layer of QDs is then applied by dip-coating over the TiO_2 surface, and the remainder of the desired TiO_2 thickness is deposited over the QDs. A SEM image of the top surface after the final TiO_2 deposition is shown in Figure 1(c). The modeled electric field for resonant modes at $\lambda = 615$ nm and $\lambda = 550$ nm are shown in Figure 1(d), demonstrating that the location of the peak electric field intensity changes with the incident wavelength within the same PC structure. By varying the depth of the QD emitters within the TiO_2 layer, and thus their proximity to the regions of highest electric field intensity, we anticipate that enhancement of the QD emission intensity will also vary. To investigate the impact of the QD placement within the TiO_2 region, we fabricated devices with the configurations described in Table I, with each batch comprised three PC samples and a flat "control" sample that was created with the same procedure, but without the periodic grating structure. The detailed fabrication procedure is described in the supplementary material.[31]

The transmission efficiency spectra of the devices were measured after each stage of the fabrication process using the test setup described in the supplementary material.[31] The minimum value of the measured transmission efficiency at normal incidence was used to determine the reported wavelength of the resonance mode. The modeled transmission efficiency for a continuous TiO_2 dielectric layer, shown as the black line in Figure 2, was normalized for the 50% effective area of the checkerboard pattern used for comparison with the measured transmission spectra.

As shown in Figure 2, each layer of deposited TiO_2 material causes a shift in the transmission efficiency minimum. There was also a shift of $\lambda = 20$–25 nm caused by the addition of the QDs observed in every sample. As listed in Table I, those structures with QDs at $t_1 = 90$ nm had the transmission efficiency minimum at $\lambda = 620$ nm. This is only $\Delta\lambda = 5$ nm greater than the $\lambda = 615$ nm value predicted by the modeled results for a continuous dielectric layer with no embedded QDs. However, for the other device conditions, the final resonance wavelengths are blueshifted from the modeled wavelength by $\Delta\lambda = 40$ nm for $t_1 = 30$ nm and by $\Delta\lambda = 20$ nm for $t_1 = 60$ nm. In these PCs, the continuous refractive index of the TiO_2 layer is disrupted and the effective refractive index of the PC is altered by the higher refractive index material of the QDs ($n = 2.5$–2.64, depending on size,[29,30]).

The impact of the QDs on the refractive index varies with their location within high or low intensity regions of the electric field, which also changes the effective refractive index of the photonic crystal. Thus, this finding is consistent with the refractive index shifts observed for QD embedded dielectrics in previous studies.[19,25]

The output intensities of the fabricated devices were also measured across a range of angles, and the impact of the QD location within the dielectric layer in relation to the enhancement of the QD emission was determined. Because the resonance is dependent on both the extraction angle and wavelength of the light coupling out of the PC, the output intensity, as shown in Figure 3, was measured across a range of angles from normal incidence (0°) to 20° at the peak QD emission of $\lambda = 615$ nm. The output intensity was averaged for the three PC structures measured in each experimental condition. The enhancement factor was determined by dividing the average QD output intensity within the PC by the planar control structure output intensity for each experimental condition. The actual enhancement factors for the checkerboard regions with

TABLE I. The thickness of each TiO_2 layer, and thus the placement of the QD layers, for each batch of test structures.

Batch	Low refractive index layer	Deposition 1 (t_1)	Emitter material	Deposition 2 (t_2)	Wavelength of transmission minima
Test 1	Replica molded polymer	30 nm TiO_2	QD	65 nm TiO_2	$\lambda = 575$ nm
Test 2	Replica molded polymer	60 nm TiO_2	QD	35 nm TiO_2	$\lambda = 595$ nm
Test 3	Replica molded polymer	90 nm TiO_2	QD	5 nm TiO_2	$\lambda = 620$ nm
Model	Replica molded polymer	95 nm TiO_2	No QDs	NA	$\lambda = 615$ nm

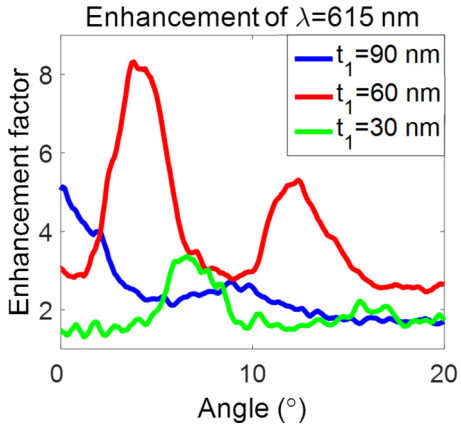

FIG. 3. The enhancement factors for the QD emission at $\lambda = 615$ nm, which were calculated by normalizing the emission from each test condition to planar with identical fabrication steps. The location of the QD layer in the structure affects both the intensity and angular output of the measured emission. The largest enhancement occurred for QDs embedded at $t_1 = 60$ nm within the TiO_2 layer; however, the only enhancement factor at normal incidence occurred at $t_1 = 90$ nm.

a resonance matched to the emission wavelength of the QD will actually be 2 times higher than the values we report here, because the QD emission in the alternate checkerboard regions are not enhanced.

The results in Figure 3 clearly show that the depth of the embedded QDs within the dielectric layer of photonic crystals impacts the enhancement of the QD emission. The highest enhancement factor at normal incidence was 5 times and occurred in the structure with a QD layer closest to the TiO_2 surface, placed at a depth $t_1 = 90$ nm. This is expected from the modeled results for $\lambda = 615$ nm light extracted at normal incidence, shown in Figure 1(d), where the greatest electric field is concentrated along the top surface of the high refractive index layer. However, the enhancement peaks diverge with the outcoupling along the guided modes of the PCs as the resonance conditions are altered by the varied effective refractive index values of the PC test conditions. Thus, the other fabricated structures demonstrated higher enhancement factors (up to 8 times) at an extraction angle of 4° for QDs placed at $t_1 = 60$ nm of TiO_2, and 7° for QDs at $t_1 = 30$ nm.

The varied angle at which the peak enhancement occurs indicates that the depth placement of emitters within PCs can be used to control both the intensity and angular output of emitted photons. This methodology would be useful to simultaneously enhance multiple QD emission wavelengths embedded at different locations within the PC structure and create tailored lighting outputs. Placement of QDs at multiple depths could also be used to specifically control the angular output of specific wavelengths, creating wide angle viewing that is desirable for screens and shared displays, or a targeted, narrowly angled output to provide privacy or depth perception for the viewer.

Using the dip-coating procedure presented in this work, we have demonstrated that varying the location of QD emitters within the high refractive index region of a PC structure can be used to tailor the enhancement and extraction angle of emitted photons. The peak enhancement values range from 3 to 8 times, depending on both the depth of the QD placement and the extraction angle of the photonic crystal coupled emission. In addition, the depth of the embedded QDs affect the effective refractive index of the dielectric PC layer and thus the enhancement factors produced by the device, adding an additional design parameter that must be considered early in the design process in order to produce the desired output enhancements.

The authors are grateful for the support of Dow Chemical Company under Research Agreement No. #226772AC.

[1]E. Yablonovitch and T. J. Gmitter, Phys. Rev. Lett. **63**, 1950 (1989).
[2]R. Magnusson and S. S. Wang, Appl. Phys. Lett. **61**, 1022 (1992).
[3]I. D. Block, L. L. Chan, and B. T. Cunningham, Microelectron. Eng. **84**, 603 (2007).
[4]L. Chen, W. Zhou, Z. Qiang, and G. J. Brown, Proc. SPIE **2006**, 63701I–63701I-7.
[5]C. Wiesmann, K. Bergenek, N. Linder, and U. T. Schwarz, Laser Photonics Rev. **3**, 262 (2009).
[6]A. David, T. Fujii, E. Matioli, R. Sharma, S. Nakamura, L. Charles, F. De, and B. Orsay, Proc. SPIE **2006**, 6115.
[7]Y. R. Do, Y. C. Kim, Y.-W. Song, C.-O. Cho, H. Jeon, Y.-J. Lee, S.-H. Kim, and Y.-H. Lee, Adv. Mater. **15**, 1214 (2003).
[8]W. H. Koo, W. Youn, P. Zhu, X.-H. Li, N. Tansu, and F. So, Adv. Funct. Mater. **22**, 3454 (2012).
[9]P. Lodahl, A. Floris Van Driel, I. S. Nikolaev, A. Irman, K. Overgaag, D. Vanmaekelbergh, and W. L. Vos, Nature **430**, 654 (2004).
[10]M. R. Singh, C. Racknor, and D. Schindel, Appl. Phys. Lett. **101**, 051115 (2012).
[11]D. Englund, D. Fattal, E. Waks, G. Solomon, B. Zhang, T. Nakaoka, Y. Arakawa, Y. Yamamoto, and J. Vuckovic, Phys. Rev. Lett. **95**, 013904 (2005).
[12]N. Ganesh, W. Zhang, P. C. Mathias, E. Chow, J. A. N. T. Soares, V. Malyarchuk, A. D. Smith, and B. T. Cunningham, Nat. Nanotechnol. **2**, 515 (2007).
[13]N. Ganesh, I. D. Block, P. C. Mathias, W. Zhang, V. Malyarchuk, and B. T. Cunningham, Opt. Express **16**, 21626 (2008).
[14]M. Kahl, T. Thomay, V. Kohnle, K. Beha, M. Hagner, A. Halm, J. Ziegler, T. Nann, Y. Fedutik, U. Woggon, M. Artemyev, A. Leitenstorfer, and R. Bratschitsch, Nano Lett. **7**, 2897 (2007).
[15]W. A. Saunders, K. J. Vahala, H. A. Atwater, and R. C. Flagan, J. Appl. Phys. **72**, 806 (1992).
[16]D. Goldberg and V. M. Menon, Appl. Phys. Lett. **102**, 081119 (2013).
[17]P. Dimitrakis, P. Normand, C. Bonafos, E. Papadomanolaki, and E. Iliopoulos, Appl. Phys. Lett. **102**, 053117 (2013).
[18]S. Prucnal, M. Turek, K. Gao, S. Zhuo, K. Pyszniak, A. Drozdziel, J. Zuk, and W. Skorupa, in *Proceedings of the IX International Conference ION 2012* (Kazimierz Dolny, Poland, 2013), pp. 935–938.
[19]X. Li, F. He, G. Liu, Y. Huang, C. Pan, and C. Guo, Mater. Lett. **67**, 369 (2012).
[20]H. Kurisu, J. Horie, K. Nagoya, S. Yamamoto, and M. Matsuura, Int. J. Mod. Phys. B **15**, 3841 (2001).
[21]K.-S. Cho, E. K. Lee, W.-J. Joo, E. Jang, T.-H. Kim, S. J. Lee, S.-J. Kwon, J. Y. Han, B.-K. Kim, B. L. Choi, and J. M. Kim, Nat. Photonics **3**, 341 (2009).
[22]Z. Zeng, E. Paspalakis, C. S. Garoufalis, and A. F. Terzis, J. Appl. Phys. **113**, 054303 (2013).
[23]X. Song, M. Wang, T. Xing, J. Deng, J. Ding, and Z. Yang, J. Power Sources **253**, 17 (2014).
[24]C. Liu, Y. Li, W. Li, J. Zhu, J. Li, Q. Chen, and Y. Yang, Mater. Lett. **120**, 170 (2014).
[25]S. P. P. Anchala and K. C. Mathur, J. Appl. Phys. **110**, 114320 (2011).
[26]V. L. Colvin, M. C. Schlamp, and A. P. Alivisatos, Nature **370**, 354 (1994).
[27]N. Ganesh, P. C. Mathias, W. Zhang, and B. T. Cunningham, J. Appl. Phys. **103**, 083104 (2008).
[28]G. G. See, L. Xu, M. S. Naughton, T. Tang, Y. Bonita, J. Joo, P. Trefonas, K. Deshpande, P. J. A. Kenis, R. G. Nuzzo, and B. T. Cunningham, Appl. Opt. **54**, 2302 (2015).
[29]N. A. Hamizi and M. R. Johan, Int. J. Electrochem. Sci. **7**, 8458 (2012).
[30]P. V. Braun and P. Wiltzius, Nature **402**, 603 (1999).
[31]See supplementary material at http://dx.doi.org/10.1063/1.4948379 for additional details regarding device fabrication and testing.